LAWRENCE
LIVERMORE
NATIONAL
LABORATORY

UCRL-JRNL-203761

Tuning electronic properties of novel metal oxide nanocrystals using interface interactions: MoO3 monolayers on Au(111)

S.-Y. Quek, M. M. Biener, J. Biener, C. M. Friend, E. Kaxiras

April 26, 2004

SURFACE SCIENCE

29 April 2004

Submitted to Nature Materials

Tuning electronic properties of novel metal oxide nanocrystals using interface interactions: MoO_3 monolayers on Au(111)

Su-Ying Quek[1], Monika M. Biener[1,2], Juergen Biener[3,5], Cynthia M. Friend[1,2], and Efthimios Kaxiras[1,4]

[1]Division of Engineering and Applied Sciences,

[2]Department of Chemistry and Chemical Biology,

[3]Center for Imaging and Mesoscale Structures, and [4]Department of Physics

Harvard University, 12 Oxford Street, Cambridge, Massachusetts 02138-2902, USA

Correspondence should be addressed to

C.M.F.: phone: (1)-(617) 495 4052, fax: (1)-(617) 496 8410,

e-mail: friend@chemistry.harvard.edu,

or, E.K.: e-mail: kaxiras@cmt.harvard.edu

[5] Current affiliation: Nanoscale Synthesis and Characterization Laboratory,

Lawrence Livermore National Laboratory,

7000 East Ave, Livermore, California 94550 USA

Abstract

Metal oxide nanocrystals deposited on metal surfaces have novel electronic properties due to interface[1,2] and nanoscale[3] effects. Crystals and nanoscale ribbons of MoO_3 are highly effective catalysts[4] and field emitters[3]. This renders MoO_3 an interesting prototype. Whilst MoO_3 exists as bilayers in the bulk crystal[5], in this work, monolayer MoO_3 nanocrystals were grown epitaxially on Au(111). *Ab initio* calculations reveal that Au stabilizes the MoO_3 monolayer through electronic charge redistribution at the interface. The Mo-O bonds are able to rotate about one another, allowing the MoO_3 monolayer to adjust to the Au lattice. As a result, the monolayer is semimetallic, unlike bulk MoO_3 which is semiconducting. This remarkable flexibility of the oxide lattice suggests the possibility of tuning electronic properties of transition metal oxides *via* interface interactions. The overall surface pattern obtained is affected by an interplay between the Au(111) surface reconstruction and the edges of the deposited MoO_3 islands.

Main text

MoO_3 nanocrystals were grown on Au(111) surfaces by both chemical vapour deposition (CVD) and physical vapour deposition (PVD) of Mo, followed by thermal oxidation. High resolution scanning tunneling microscopy (STM) and low energy electron diffraction (LEED) studies indicate that the MoO_3 islands grown by either technique have a c(4 × 2) unit cell. STM images further reveal that the islands are one monolayer in height, i.e. half of the bilayer found in bulk MoO_3. This interesting surface structure has another important ramification: although clean Au(111) reconstructs to

form a herringbone pattern[6], STM images indicate that the reconstruction is not continued under the islands (**Fig. 1**), a feature we adopt in the theoretical model of the system.

In its optimized structure (**Fig. 2a**), the MoO_3 monolayer distorts to fit the Au lattice and has distinct symmetry properties from its bulk analogue (**Fig. 2c**). In contrast to the bulk case, the MoO_3 monolayer has two non-equivalent planes of reflection and glide symmetry. The slab appears to be composed of MoO_3 units tilting alternately forwards and backwards relative to the surface normal, along the axes of reflection (**Fig. 2b**). Using the notation in **Fig. 2**, O_{b2} is situated directly above a Au atom, whilst O_{b1} is above a Au bridge site. Mo sits in a 3-fold site, off-centered away from the Au atoms below O_{b2}.

Using the electronic wavefunctions associated with this structure, we performed simulations of the STM images expected for this system, based on the Tersoff-Hamann theory[7]. The bright spots in the STM images are found to correspond to lateral positions of terminal O. Within the limits of experimental variance, the relative positions of these spots are the same in theory and experiment (**Fig. 3**), thus lending strong evidence to the tilting of MoO_3 units described above.

Phonon frequencies of the MoO_3 monolayer were computed at the Brillouin zone center, using the harmonic approximation. To compare these with frequencies from electron energy loss spectroscopy (EELS), selection rules based on both dipole and impact scattering[8] were employed. We found only 6 EELS-active phonon modes out of 24 possible ones. The calculated frequencies, with corresponding experimental values in parentheses, are, in cm^{-1}: 1030, 1020 (990), 804 (850), 430 (480), 351 (280) and 160 (-). Noting that instrument resolution is about 80 cm^{-1}, and that 160 cm^{-1} is out of the

detection range, theoretical and experimental frequencies correspond fairly well, especially given that finite-size effects were neglected in the simulation. This correspondence provides further evidence for the predicted symmetry properties.

The preceding results confirm unequivocally that the optimized structure matches the experimental structure of the interior of the MoO_3 monolayer islands on Au(111), without including defects. It is remarkable that the Mo-O bonds have sufficient freedom to rotate about one another, to allow a distortion of the MoO_3 monolayer from the bulk, so as to adjust to the Au lattice. Geometrical considerations indicate that the c(4 × 2) unit cell is in fact the smallest unit cell for which epitaxy can be achieved, if sufficient bonding between Mo atoms through the bridging O bonds is to be preserved. Moreover, the symmetry properties of the MoO_3 monolayer are dictated by the symmetries of the Au substrate – the reflection symmetry in the oxide is matched by a reflection symmetry in the Au lattice, and the glide plane symmetry in the oxide corresponds to a similar symmetry in the top Au layer, if its relation to underlying Au layers is ignored.

Unlike semiconducting bulk MoO_3, the MoO_3 monolayer is semimetallic, as deduced from the density of states (DOS) of the MoO_3/Au system, projected onto the oxide slab. The MoO_3 slab alone has a similar, semimetallic DOS. However, if this slab is allowed to relax in the same unit cell without Au, it becomes semiconducting. The relaxed slab resembles an interacting array of trigonal-pyramidal MoO_3 molecules: rows of Mo atoms relax alternately towards rows of O_{b1} and O_{b2}, thus breaking the glide-plane symmetry. This symmetry-breaking, accompanied by the semimetal-to-insulator transition, suggests that the slab undergoes a Jahn-Teller distortion when allowed to relax as above. Analysis of the DOS of the semimetallic MoO_3 slab reveals that Fermi level

states are localized in the plane of Mo and bridging O. It is therefore likely that a semimetal-to-insulator transition occurs because symmetry-degenerate states at the Fermi level split to form bonding and anti-bonding states, when Mo relaxes towards a pair of bridging O atoms to form stronger bonds.

The above analysis suggests that the semimetallic character of the MoO_3 monolayer on Au is related to the glide plane symmetry in the oxide layer and can be attributed at least in part to the strained Mo-O bridging bonds. The difference in energy between the relaxed MoO_3 slab and the MoO_3 slab strained to fit the Au lattice, was calculated to be 0.15 eV/unit cell. On the other hand, the cohesive energy for the MoO_3/Au system, with respect to a relaxed unreconstructed Au(111) surface and the isolated frozen MoO_3 slab, was calculated to be –0.24 eV/unit cell. The energy cost of straining the MoO_3 slab is therefore overcome by the gain in cohesive energy upon formation of the MoO_3/Au interface. In order to elucidate the nature of the MoO_3/Au interaction, we plot the difference between the charge density of the MoO_3/Au system, and the sum of charge densities of isolated MoO_3 and Au slabs, frozen in configuration from the joint system (**Fig. 4**). This reveals that the MoO_3 slab induces an electronic charge redistribution above the Au surface. The positively-charged Mo ions draw electron density to the region directly underneath them. Each of these electron clouds is in turn attracted by the nearest Au atom, since Au surface atoms are electron-deficient. In this way, Mo is drawn closer to the Au atom nearest to it. On the other hand, the partial negative charges on O_{b2} cause them to be attracted to Au atoms directly beneath them. These interactions together cause the Mo-O_{b2} bridging bonds to strain resulting in semimetallic character. The electronic charge redistribution satisfies local bonding

requirements, which allows the Au surface to act as the other half of the MoO_3 bilayer. The MoO_3 monolayer in turn stabilizes the Au(111) surface, with each Au atom bonded either to an O atom (O_{b2}) or a Mo atom, and as a result, the surface reconstruction under the MoO_3 islands is lifted.

In-situ STM studies suggest that the MoO_3 islands grow *via* aggregation of MoO_3 molecular species. Earlier theoretical work has shown that induced electrostatic interactions increase the cationic character of Mo, as MoO_3 units build up to form bulk MoO_3[9]. Similarly, in our calculations, the local charge on Mo is larger in the MoO_3 slab on Au than in a single MoO_3 molecule. The increased ionic character upon aggregation of MoO_3 molecular species allows the oxide to polarize the electron gas at the MoO_3/Au interface. Charge redistribution at the interface stabilizes the islands, allowing nucleation and growth. The surface of these islands corresponds to the natural cleavage plane of bulk MoO_3 and has a free energy[10] of only 0.05-0.07 J/m^2. In contrast, Au has a surface free energy[11] of 1.62 J/m^2. Growth of the MoO_3 monolayer is thus driven by both a gain in interface energy and a reduction in surface free energy.

Interestingly, the long straight edges of the ensuing islands run along the ⟨11-2⟩ directions of Au, parallel to the herringbone pattern, and not the ⟨-312⟩ directions, diagonal to the c(4 × 2) unit cell, along which MoO_3 units are close-packed (**Fig. 2a**). The herringbone pattern is aligned parallel to straight island edges, but tends to form sharp bends at rough island edges (**Fig. 1**). The herringbone pattern has the property of soliton-waves[12]; therefore, absence of Au reconstruction beneath the islands imposes hard-wall boundary conditions on these waves, causing the herringbone pattern to be oriented so that it is locally parallel to the island edges. The distinct correlation between

straight island edges and the herringbone direction suggests that there is an interplay between the herringbone structure and the MoO_3 islands that affects the overall pattern that develops on the surface. Further theoretical and experimental investigation of kinetic effects will substantially clarify this picture.

Discussion

The growth of oxide thin films on metals has attracted considerable attention because enhanced chemical activity has been observed in some of these systems, and additional novel properties are expected to arise from the image potential screening of charge fluctuations in the oxide, and from interface hybridization or charge transfer effects[2]. In this work, we have demonstrated that whilst MoO_3 exists as bilayers in the bulk crystal, MoO_3 monolayer nanocrystals can be grown on the Au(111) surface. The Au surface acts as the other half of the MoO_3 bilayer, stabilizing the MoO_3 monolayer *via* electronic charge redistribution and energetic gains due to interface formation and reduction of the surface energy of Au. We have shown that the Mo-O bonds have sufficient freedom to rotate about one another, allowing the MoO_3 monolayer to adjust to the Au substrate. The resulting epitaxial strain gives the oxide semimetallic character. We expect that this substantial rotational degree of freedom, of oxide bonds about one another, is common to many transition metal oxides, especially those that have more than one structural phase in the bulk. Thin films of some of these oxides have been successfully grown on metal surfaces[13]. In fact, it is likely that the growth mechanism proposed herein is general enough so that a rich variety of other novel structures of such oxides can be grown on metal surfaces by condensing molecular species, which become increasingly ionic, interacting with the substrate to create a wetting oxide layer. Our

results suggest that the metallic substrate may be used as a handle to tune the electronic properties of these oxide structures, by exploiting the flexibility of the oxide lattice, and the polarizability of the interface electron gas.

Methods

Experimental details:

Nanocrystalline MoO_3 islands on Au(111) were prepared in two different ultra-high vacuum systems, and full experimental details are provided in reference [14] and the following submitted paper: M.M.B., J.B., R. Schalek, & C.M.F. Growth of nanocrystalline MoO_3 on Au(111) studied by *in-situ* STM. Briefly, Mo deposited on Au(111) via CVD was oxidized by exposure to NO_2. Only small amounts of Mo were deposited and oxidized at a time to allow full oxidation. Typically, the surface was exposed to 1 L of $Mo(CO)_6$ and 10 L NO_2 alternatively at 450 K, followed by annealing to 600 K for 1 min after every four cycles of dosing, for a total of 16 cycles (**Fig. 3a**). Mo deposited via PVD was oxidized by subsequent exposure to NO_2. For example, 0.3 ML Mo deposited on Au(111) at 600 K were oxidized by exposure to 20 L NO_2 at 600 K (**Fig. 1**). STM images shown in this paper were collected at room temperature.

Details of calculations:

The density functional calculations employed the projected augmented wave method[15,16] and the Perdew-Wang 91 gradient correction[17] for the exchange-correlation functional, as implemented in the VASP[18] code. The optimized structure of bulk MoO_3 obtained with this approach compared well to the known crystal structure, with bond lengths accurate to 1-3%. We model the Au(111) surface by a slab of 6 Au layers,

separated by 16.5 Å of vacuum before the oxide is introduced. The MoO_3 monolayer and the top 3 Au layers were allowed to relax until the forces on atoms in these layers were less than 0.01 eV/Å. Geometry optimizations were performed using a plane-wave energy cutoff of 400 eV and a 3 × 3 *k*-point mesh. Increasing the mesh density to 6 × 6 did not change the optimized geometry of the MoO_3 monolayer on Au significantly. Energies and charge densities were calculated using a plane-wave cutoff of 500 eV and a 12 × 12 *k*-point mesh. Such a mesh was sufficient for the convergence of the total energy in a bulk-terminated Au(111) surface.

Acknowledgements

The calculations were performed on the National Computational Science Alliance IBM P690, under DMR030044. The experimental work was supported by the National Science Foundation, under the Harvard Nanoscale Science and Engineering Center, PHY-011-7795, and the Harvard Materials Research Science and Engineering Center, DMR-0213805, as well as the Department of Energy, Basic Energy Sciences, under FG02-84-ER13289. J.B. acknowledges current support under the auspices of the U. S. Department of Energy by the University of California, Lawrence Livermore National Laboratory under Contract No. W-7405-Eng-48. The authors thank D.-H. Kang and X. Deng for work on EELS and XPS respectively. S.-Y.Q. thanks the Singapore Agency for Science, Technology and Research for a graduate fellowship.

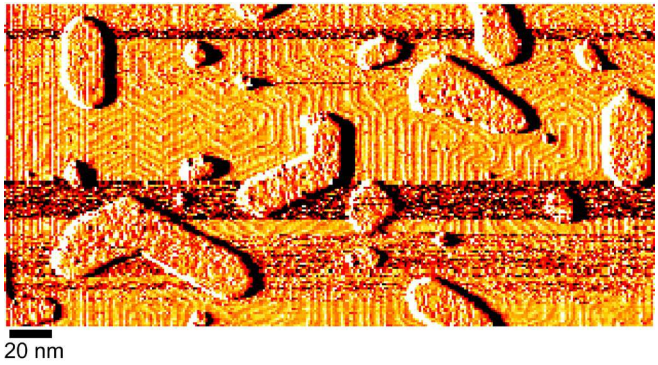

Figure 1. STM image of MoO_3 islands on Au(111). The Au herringbone reconstruction runs parallel to the straight island edges, and bends sharply at rough island edges. These bends indicate that the Au(111) reconstruction is lifted under the MoO_3 islands.

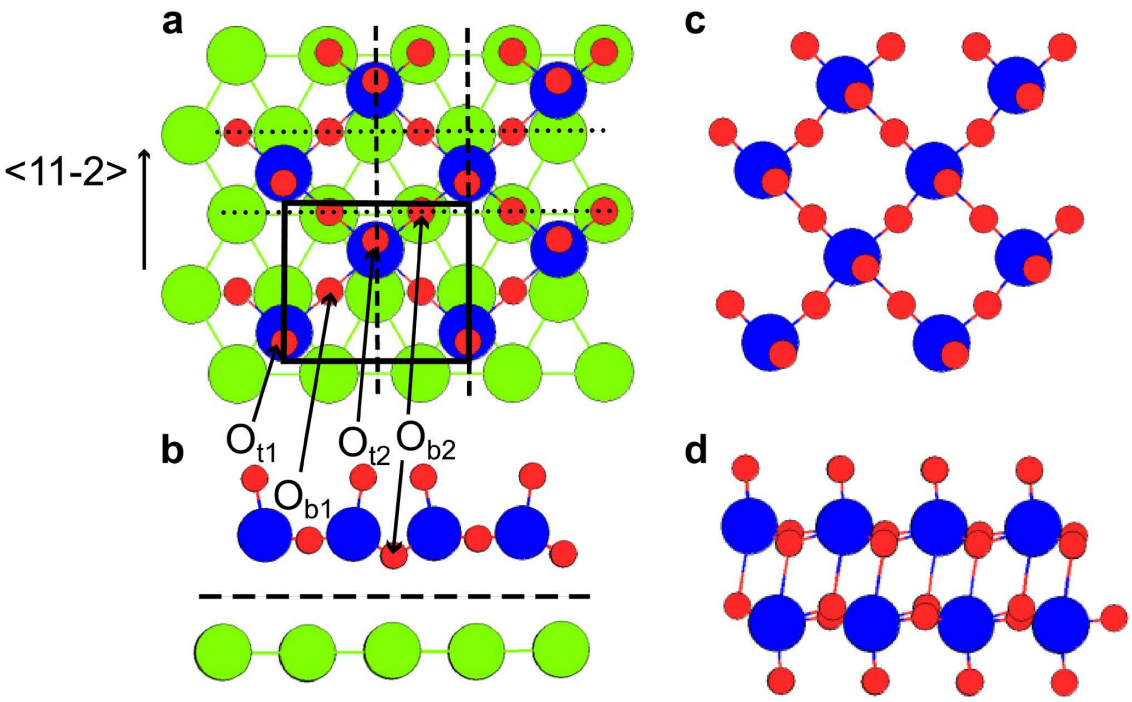

Figure 2. Atomic structure of MoO_3 slabs. a, Top view of MoO_3 monolayer on Au. **b**, Side view of MoO_3 monolayer on Au. **c**, Top view showing half a bulk MoO_3 bilayer. **d**, Side view of a bulk MoO_3 bilayer. Blue, red and green circles represent Mo, O and Au atoms respectively. MoO_3 units are close-packed along the diagonal of the c(4 × 2) unit cell, indicated by the black box. Dashed and dotted lines in **a** respectively denote planes of reflection and glide symmetry in the oxide monolayer. The view in **b** is that down the glide planes, and shows MoO_3 units tilting backwards and forwards along the axes of reflection. O_{b1} and O_{b2} denote the two inequivalent bridging O atoms in the unit cell, with O_{b2} nearer to the Au surface than O_{b1}. The mirror images of O_{b1} and O_{b2} in the planes of reflection symmetry are not labelled. The terminal O atoms are labelled O_{t1} and O_{t2}. The ⟨11-2⟩ crystallographic direction of Au, parallel to the herringbone reconstruction, is indicated in **a**. The dashed line in **b** denotes the plane relevant for the plot in **Fig. 4**.

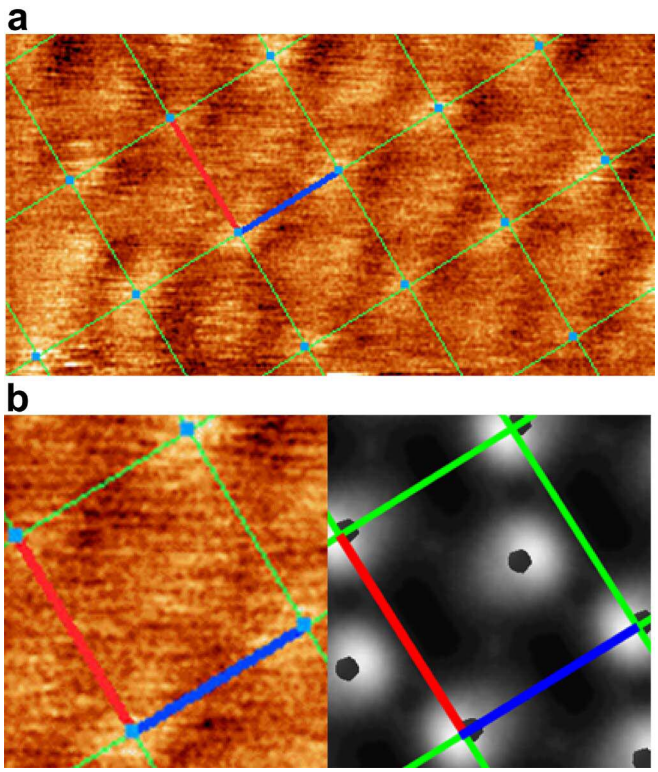

Figure 3. STM images of the interior of the MoO_3 islands. a, Experimental STM image. **b**, **Left:** Close-up section of experimental STM image in **a**. **Right:** STM simulation corresponding to a tip-sample separation of 1.4 Å. The sample bias voltages were –0.580 V in both the experiment and the simulation. A brighter color represents a more intense current. The green lines show the c(4 × 2) unit cells. The bright spots in the experimental images are related to lateral positions of terminal O atoms on the surface, which are marked by black pentagons in the simulation. In each cell, there is a bright spot slightly off-center. In polar co-ordinates with respect to the (x, y) axes (denoted as blue and red in the figure), the off-center spot is at r = 4.3 Å, θ = 42 ° in the simulation, and r = 4.1 ± 0.4 Å, θ = 43 ± 4 ° in the experiment.

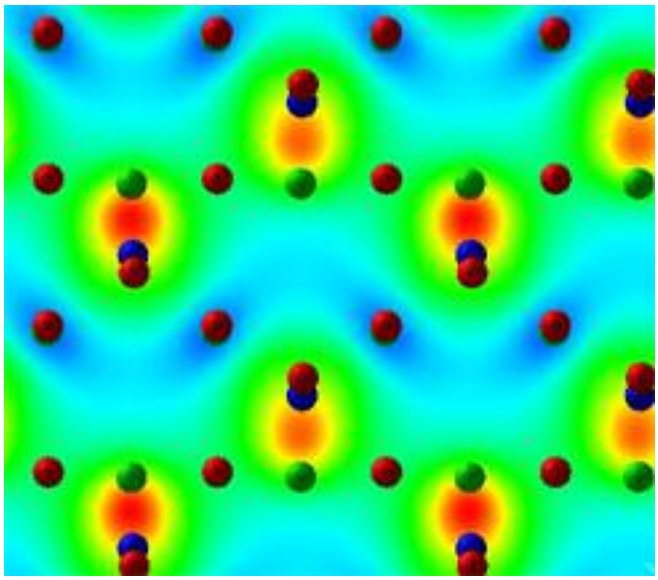

Figure 4. Charge density difference between the MoO_3/Au system and the sum of charge densities of isolated MoO_3 and Au slabs, frozen in configuration from the joint system. The values are those on a plane mid-way between MoO_3 and Au, as indicated by the dashed line in **Fig. 2b**. Blue, red and green spheres denote the lateral positions of Mo, O and Au atoms respectively. Half the Au atoms are hidden directly under O_{b2}. Blue regions, corresponding to charge depletion, occur below O_{b2}, and red regions, corresponding to charge accumulation, are seen between Mo and the nearest Au atoms. Values of the charge density difference range from –0.0093 e/Å^3 to 0.0133 e/Å^3.

References

1. Sinnott, S. B. & Dickey, E. C. Ceramic/metal interface structures and their relationship to atomic- and meso-scale properties. *Mater. Sci. Eng. R-Rep.* **43**, 1-59 (2003).
2. Altieri, S., Tjeng, L. H. & Sawatzky, G. A. Ultrathin oxide films on metals: new physics and new chemistry? *Thin Solid Films* **400**, 9-15 (2001).
3. Wang, Z. L. Functional Oxide Nanobelts: Materials, Properties and Potential Applications in Nanosystems and Biotechnology, doi: 10.1146/annurev.physchem.55.091602.094416. *Annu. Rev. Phys. Chem.* (2004).
4. Haber, J. & Lalik, E. Catalytic properties of MoO_3 revisited. *Catal. Today* **33**, 119-137 (1997).
5. Kihlborg, L. Least squares refinement of the crystal structure of molybdenum trioxide. *Arkiv Kemi* **21**, 357-364 (1963).
6. Barth, J. V., Brune, H., Ertl, G. & Behm, R. J. Scanning tunneling microscopy observations on the reconstructed Au(111) surface: Atomic structure, long-range superstructure, rotational domains, and surface defects. *Phys. Rev. B* **42**, 9307-9318 (1990).
7. Tersoff, J. & Hamann, D. R. Theory and Application for the Scanning Tunneling Microscope. *Phys. Rev. Lett.* **50**, 1998-2001 (1983).
8. Ibach, H. & Mills, D. L. *Electron Energy Loss Spectroscopy and Surface Vibrations.* (Academic Press, New York, NY, 1982).

9. Papakondylis, A. & Sautet, P. *Ab Initio* Study of the Structure of the alpha-MoO_3 Solid and Study of the Adsorption of H_2O and CO Molecules on Its (100) Surface. *J. Phys. Chem.* **100**, 10681-10688 (1996).

10. Overbury, S. H., Bertrand, P. A. & Somorjai, G. A. The Surface Composition of Binary Systems. Prediction of Surface Phase Diagrams for Solid Solutions. *Chem. Rev.* **75**, 547-560 (1975).

11. Mezey, L. Z. & Giber, J. The Surface Free Energies of Solid Chemical Elements: Calculation from Internal Free Enthalpies of Atomization. *Jpn. J. Appl. Phys.* **21**, 1569-1571 (1982).

12. El-Batanouny, M., Burdick, S., Martini, K. M. & Stancioff, P. Double-Sine-Gordon Solitons: A Model for Misfit Dislocations on the Au(111) Reconstructured Surface. *Phys. Rev. Lett.* **58**, 2762-2765 (1987).

13. Chambers, S. A. Epitaxial growth and properties of thin film oxides. *Surf. Sci. Rep.* **39**, 105-180 (2000).

14. Biener, M. M. & Friend, C. M. Heteroepitaxial growth of novel MoO_3 nanostructures on Au(111). *Surface Science Letters* (accepted).

15. Kresse, G. & Joubert, J. From ultrasoft pseudopotentials to the projector augmented wave method. *Phys. Rev. B* **59**, 1758-1775 (1999).

16. Blochl, P. E. Projector augmented-wave method. *Phys. Rev. B* **50**, 17953-17979 (1994).

17. Perdew, J. P. & Wang, Y. Accurate and simple analytic representation of the electron-gas correlation energy. *Phys. Rev. B* **45**, 13244-13249 (1992).

18. Kresse, G. & Furthmuller, J. Efficient iterative schemes for *ab initio* total-energy calculations using a plane-wave basis set. *Phys. Rev. B* **54**, 11169-11186 (1996).